Korean J. Chem. Eng., 32(7), 1258-1266 (2015)
DOI: 10.1007/s11814-014-0319-5

pISSN: 0256-1115
eISSN: 1975-7220

Synthesis and physicochemical characterization of ZrO_2-doped NiMo/Al_2O_3 nanocatalyst via precipitation and sequential impregnation methods used in hydrodesulfurization of thiophene

Parisa Jabbarnezhad[*,], Mohammad Haghighi[*,**,†], and Parisa Taghavinezhad[*,**]**

*Chemical Engineering Faculty, Sahand University of Technology, P. O. Box 51335-1996, Sahand New Town, Tabriz, Iran
**Reactor and Catalysis Research Center (RCRC), Sahand University of Technology,
P. O. Box 51335-1996, Sahand New Town, Tabriz, Iran
(*Received 22 April 2014 • accepted 28 October 2014*)

Abstract−A series of Al_2O_3-ZrO_2 composite with various ZrO_2 contents were prepared by precipitation and NiMo was dispersed over them via sequential impregnation. The samples were characterized by XRD, FESEM, EDX, BET, TPR-H_2 and FTIR techniques. XRD patterns indicate the homogeneous dispersion of ZrO_2 on Al_2O_3 in small amounts of ZrO_2. Comparison of FESEM images implies that with the incorporation of small amounts of ZrO_2 (5, 12 and 17 wt%) on Al_2O_3, the catalyst morphology changed from large ensembles to smaller particles with uniform distribution. According to TPR-H_2 profiles, adding ZrO_2 increases the reducibility of nanocatalysts. Catalytic activity results showed that the NiMo over Al_2O_3-ZrO_2 composite showed higher hydrodesulfurization activity than that of Al_2O_3 supported catalyst. The maximum of hydrodesulfurization activity was observed for NiMo/Al_2O_3-ZrO_2 nanocatalyst with 12 wt% of ZrO_2 content related to enhanced physicochemical properties.

Keywords: NiMo/Al_2O_3-ZrO_2, Precipitation, Sequential Impregnation, Hydrodesulfurization, Thiophene

INTRODUCTION

Improvement of the performance of hydrodesulfurization (HDS) catalysts is necessary to comply with the new worldwide strict environmental legislations concerning sulfur content in fuels [1]. To achieve this goal, many approaches were experimented, among which the variation of support composition that could be one of the most promising routes [2,3]. It is well-documented that the support has a basic role in determining the nature and the number of active sites and consequently catalytic performances [4,5].

The basic composition of traditional HDS catalysts is composed of molybdenum sulfide promoted by cobalt or nickel on γ-Al_2O_3 [6]. The active sites in these types of catalysts are represented by (Co)NiMoS, Ni_3S_2, Co_9S_8 structure in which nickel (cobalt) atoms are located at the edges of MoS_2 slabs [7]. Due to its outstanding textural and mechanical properties and relatively low cost, γ-alumina is the most widely used support for HDS catalysts [8-10]. However, due to the existence of undesirable strong interactions between active phase and support, a major part of the research is focused on development of HDS catalyst support with new materials [11]. Many studies have shown that variations in metal-support interactions influence the formation of the (Co)NiMoS, Ni_3S_2, Co_9S_8 active phases and their dispersion over the support surface. Furthermore, the reducibility and sulfidability of the deposited metal oxides can be influenced [12,13].

Different materials have been used as supports for HDS catalysts, namely, zirconia [14-16], titania [17,18], carbon [19,20], mesoporous materials like MCM-41 [21,22], SBA-15 [23], etc. Among these supports, ZrO_2 has attracted great attention due to its high redox properties and promising activity [24]. However, its low surface area and high price make this support unsuitable for industrial applications [25]. To overcome these drawbacks, increasing attention has been given to the development of mixed oxide supports by combining the higher surface areas and thermal stability of Al_2O_3 with the unique properties of ZrO_2 [26]. Catalysts supported on Al_2O_3-ZrO_2 were found to be more active than pure alumina in HDS reaction. Zhang and coworkers [27] prepared Al_2O_3-ZrO_2 composite oxides and investigated the HDS performance of diesel oil on the sulfided NiMo/Al_2O_3-ZrO_2 catalyst. They reported a significant increase in the NiMo dispersion with incorporation of ZrO_2 into the support. Furthermore, they reported binary oxide-supported catalysts exhibit higher and easier reducibility in comparison to alumina supported ones. Their HDS results illustrated that NiMo/Al_2O_3-ZrO_2 catalyst with optimum ZrO_2 contents exhibited much higher catalytic activities than that of Al_2O_3-supported catalyst. They have shown with ZrO_2 content of 15 wt%, the NiMo/Al_2O_3-ZrO_2 catalyst presented the highest HDS activity, which was consistent with its textural properties and the large amounts of Lewis acid sites. Li and coworkers [28,29] investigated the HDS activity of dibenzothiophene (DBT) on sulfided CoMo/Al_2O_3-ZrO_2 catalyst. In result, CoMo/Al_2O_3-ZrO_2 catalyst with suitable ZrO_2 content (12.1 wt%) was the most active catalysis for HDS of dibenzothiophene. They observed a multilayered active structure for mixed oxide supported catalyst and mono-layered low active structure for Al_2O_3-supported catalyst. Unlike the Al_2O_3-TiO_2 system which has been studied widely and thoroughly for its commercial brightening prospects [30-32],

†To whom correspondence should be addressed.
E-mail: haghighi@sut.ac.ir

the zirconia supported catalysts have shown higher intrinsic activity in HDS reactions.

The physicochemical properties of the synthesized catalyst can be influenced by preparation method [33-35]. The reported literature has shown that the precipitation method could enhance the catalyst properties like surface area, morphology and particle size [36-38]. To explore further insight into the effect of zirconia on HDS activity of supported catalysts, in the present work zirconia-doped alumina supports were prepared by precipitation method and NiMo was dispersed over support via sequential impregnation method. X-ray diffraction (XRD), field emission scanning electron microscopy (FESEM), energy dispersive X-ray (EDX), nitrogen adsorption, Brunauer-Emmett-Teller (BET), H_2-temperature programmed reduction (TPR-H_2) and Fourier-transformed infrared (FTIR) techniques were employed for physicochemical characterization of the synthesized nanocatalysts. Finally, the catalytic activity of prepared catalysts was evaluated during the HDS of thiophene at 160 °C and atmospheric pressure.

MATERIALS AND METHODS

1. Materials

For the preparation of support, zirconium oxychloride ($ZrOCl_2 \cdot 8H_2O$) supplied from Aldrich and aluminum hydroxide $Al(OH)_3$ from Merck company were applied as the sources of ZrO_2 and γ-Al_2O_3, respectively. Distilled water and NH_4OH aqueous solution (Merck) were used as solvent and as precipitating agent, respectively. Ammonium heptamolybdate tetrahydrate $(NH_4)_6Mo_7O_{24} \cdot 4H_2O$) and nickel nitrate hexahydrate ($Ni(NO_3)_2 \cdot 6H_2O$ as the sources of molybdenum and nickel, respectively, were obtained from Merck and used without any further purification for the preparation of catalysts. To measure the catalytic activity, thiophene (Merck) and decane (Merck) were used as the model sulfur compound and solvent, respectively.

2. Nanocatalyst Preparation and Procedures

2-1. Al_2O_3-ZrO_2 Synthesis

A schematic flow chart for the preparation steps of Al_2O_3-ZrO_2 support by precipitation method is given in Fig. 1. The following procedures were employed for preparation of support: pseudo-boehmite and deionized water were mixed and then the required amount of $ZrOCl_2 \cdot 8H_2O$ aqueous solution was added into the above mixture while vigorous stirring for 4 h. Then, ammonia solution as precipitating agent was gradually added into the mixture until the final pH reached 8±0.2. The mixture was aged for 2 h at room temperature and was filtered and washed with required amount of distilled water to eliminate all the Cl ions. Then, the samples were dried over night at 110 °C and finally calcined at 550 °C for 4 h in air. The samples were indicated as AZx where A and Z denote the Al_2O_3 and ZrO_2, respectively, and x refers to the weight percentage of zirconium on support.

2-2. Dispersion of NiMo over Al_2O_3-ZrO_2

A schematic flow diagram for dispersion of NiMo over Al_2O_3-ZrO_2 via impregnation method is shown in Fig. 2. The calcined support was impregnated successively using required amounts of aqueous solutions of ammonium heptamolybdate, $(NH_4)_6Mo_7O_{24} \cdot 4H_2O$ and nickel nitrate, $Ni(NO_3)_2 \cdot 6H_2O$. First, Mo was impregnated, mixed for 1.5 h at 40 °C. Then Ni was impregnated while mixing for 2 h. The impregnated catalyst was dried at 110 °C overnight, and calcined in the presence of air at 550 °C for 4 h. The samples were indicated as NiMoAZx where A and Z denote the Al_2O_3 and ZrO_2, respectively, and x refers to the weight percentage of zirconium in support. All the samples were prepared with the constant amounts of Mo and Ni (corresponding to MoO_3: 17 wt% and NiO: 3.5 wt%) and the various amounts of ZrO_2 as can be seen in Table 1.

The oxidic catalysts obtained in the previous step, prior to the HDS reaction, were pre-sulfided in a stream of 10 vol% H_2S in H_2 (with a flow rate of 40 ml/min) under atmospheric pressure. This operation was performed in a glass-tubular reactor at 400 °C for 2 h. The catalyst sulfidation was done ex-situ in a glass-tubular reac-

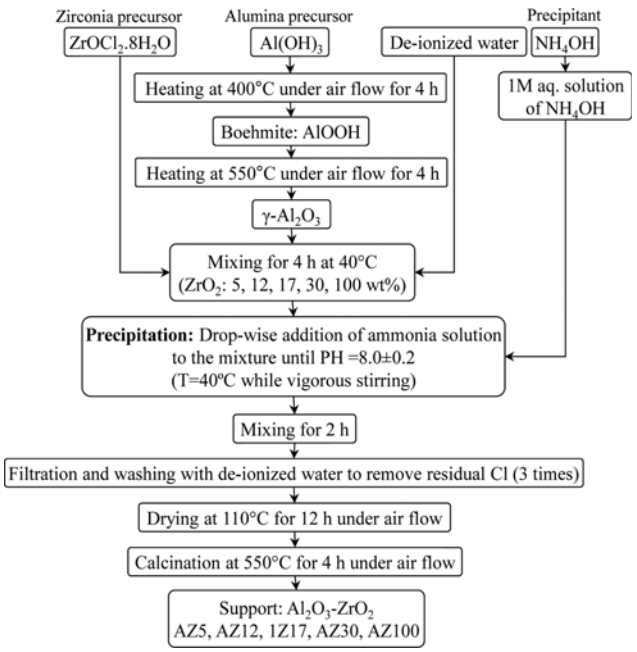

Fig. 1. Preparation steps of Al_2O_3-ZrO_2 support with different ZrO_2 loading using precipitation method.

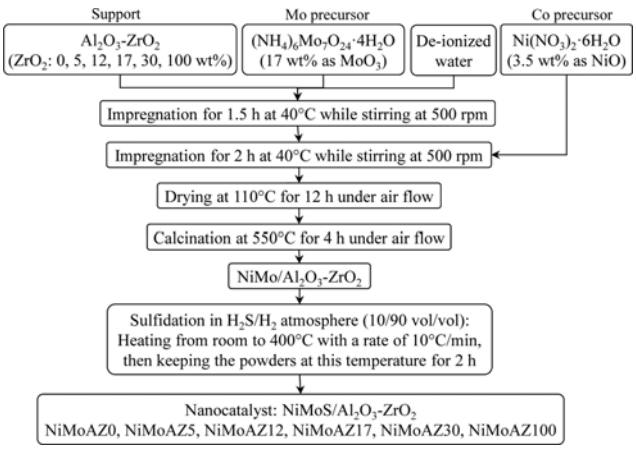

Fig. 2. Preparation steps of NiMo/Al_2O_3-ZrO_2 nanocatalysts with different ZrO_2 loading via sequential impregnation method.

Table 1. Composition and nomenclature of $NiMo/Al_2O_3$-ZrO_2 nanocatalysts with different ZrO_2 loading synthesized via sequential impregnation method

Nanocatalysts	Nomenclature	Synthesis method	NiO (%)	MoO_3 (%)	ZrO_2 (%)
$NiMo/Al_2O_3$	NiMoAZ0	Impregnation	3.5	17	0
$NiMo/Al_2O_3$-ZrO_2	NiMoAZ5	Impregnation	3.5	17	5
$NiMo/Al_2O_3$-ZrO_2	NiMoAZ12	Impregnation	3.5	17	12
$NiMo/Al_2O_3$-ZrO_2	NiMoAZ17	Impregnation	3.5	17	17
$NiMo/Al_2O_3$-ZrO_2	NiMoAZ30	Impregnation	3.5	17	30
$NiMo/ZrO_2$	NiMoAZ100	Impregnation	3.5	17	100

tor. To avoid any contact with air, the sulfided catalyst was transferred into the stirred slurry-tank reactor in an insulated system.

3. Nanocatalysts Characterization Techniques

For identification of crystallography of the synthesized nanocatalysts, XRD patterns were obtained between 2θ=10-90° using a Bruker D8 Advance diffractometer; using CuKa radiation (λ=1.54178 Å) and step rate of 0.03°/s. The morphology of the catalysts was investigated using field emission scanning electron microscopy (FESEM), Hitachi S-4160. EDX analysis was carried out by Vega\\Tescan, BSE detector for elemental analysis. BET (Brunauer, Emmett, and Teller) surface area (S_{BET}) of the samples was measured by the conventional nitrogen adsorption-desorption technique in a Quantachrome ChemBET 3000 apparatus. The reducibility of the catalysts was measured by temperature-programmed reduction of hydrogen (TPR-H_2) using a BELCAT (Japan), which included an online thermal conductivity detector (TCD). The sample was loaded into a quartz reactor and a flow of 10% H_2/Ar with 40 ml/min was passing through the samples and the temperature was being raised at a rate of 10 °C/min. Infrared analysis of the support and catalysts was carried out by a Unicam 4600 FTIR spectroscope for identification of surface functional groups.

4. Experimental Setup for Catalytic Performance Test

A schematic flow diagram of experimental setup for HDS activity tests of the sulfided nanocatalysts is shown in Fig. 3. Hydrodesulfurization of thiophene tests was performed in a stirred slurry-tank reactor (50 ml) in the liquid phase at 160 °C under atmospheric hydrogen pressure for 2 h. In each run, the reactor was charged with 30 ml of the reactant solution consisting of 1 wt% thiophene in decane and 0.2 g of sulfided catalyst. During the reaction, hydrogen flow rate was fixed at 20 ml/min. The liquid product was collected and analyzed by gas chromatography (GC Chrom, Teif Gostar Faraz, Iran) with FID detector and using a silicone capillary column

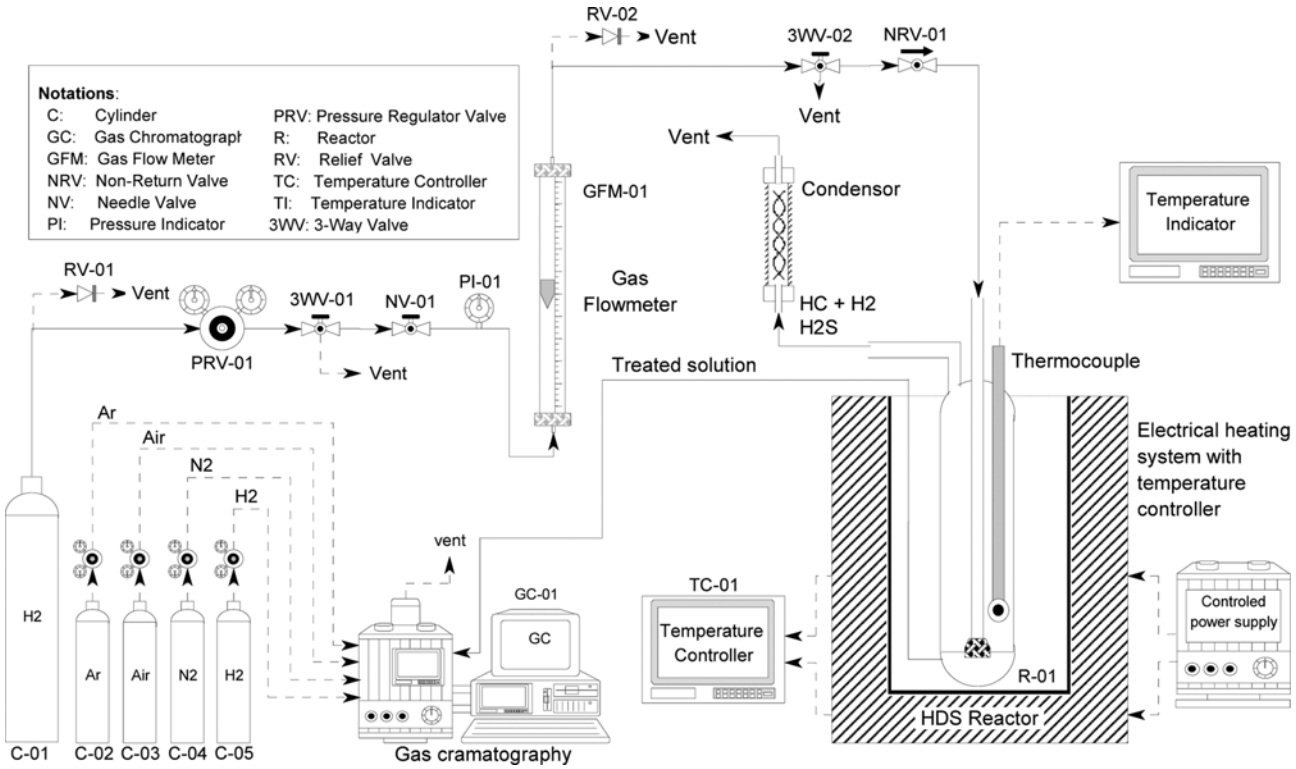

Fig. 3. Experimental setup for activity test of $NiMo/Al_2O_3$-ZrO_2 nanocatalysts with different ZrO_2 loading toward hydrodesulfurization of thiophene.

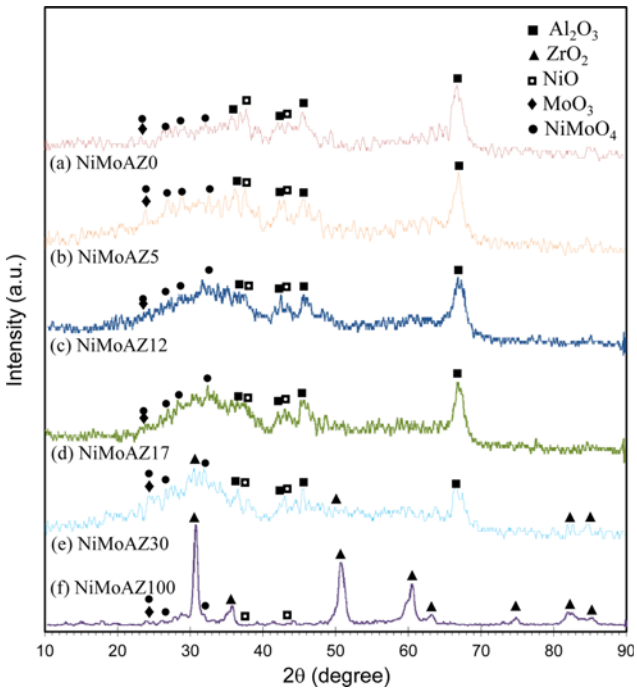

Fig. 4. XRD patterns of NiMo/Al_2O_3-ZrO_2 nanocatalysts with different ZrO_2 loading: (a) NiMoAZ0, (b) NiMoAZ5, (c) NiMo AZ12, (d) NiMoAZ17, (e) NiMoAZ30 and (f) NiMoAZ100.

(HP PLOT-Q; 0.53 mm×15 m). Note that the sampling process carried out in batch mode. To take liquid sample from the reactor, a syringe was employed.

RESULTS AND DISCUSSIONS

1. Nanocatalysts Characterization

1-1. XRD Analysis

The XRD patterns of the synthesized NiMoAZx catalysts are shown in Fig. 4. To identify the crystalline phases, XRD patterns of the samples were compared with those of Joint Committee Powder Diffraction Standards (JCPDS) data. The peaks observed at 2θ=37.4, 42.8, 45.7 and 67.3 degree in the patterns are related to presence of γ-Al_2O_3 (00-004-0880). And the intensity of these peaks is decreased with increasing of ZrO_2 contents. As can be seen in the figure, no independent lines due to crystalline ZrO_2 are observed in XRD patterns of NiMoAZ5, NiMoAZ12 and NiMoAZ17 catalysts. This may be due to the low concentration of ZrO_2 or well dispersion of this oxide in the alumina matrix in the samples. However, the XRD pattern of NiMoAZ30 showed weak peaks at 2θ=30.2 and 50.3°, which correspond to the tetragonal phase of zirconia [28]. The peaks related to tetragonal and monoclinic phases of ZrO_2 were detectable in pure zirconia-supported catalyst. This observation indicates that by doping of ZrO_2 on alumina, the monoclinic phase of ZrO_2 was eliminated and the tetragonal phase was stabilized [27]. As can be seen from XRD patterns, the peaks related to ZrO_2 in the NMAZ30 samples appeared slightly at lower 2θ. This observation indicates the progressive formation of a solid solution between Al_2O_3 and ZrO_2. According to the literature [39] the formation of solid solution between Al_2O_3 and ZrO_2 was started from x=0.2 and lasted at x=0.8.

The weak diffraction peaks attributed to the bulk MoO_3 (00-047-1081), NiO (01-073-1519) and $NiMoO_4$ (00-045-0142) active phases, were detected in NiMoAZ0, NiMoAZ5, NiMoAZ17, NiMoAZ30 and NiMoAZ100 that are poorly crystalline. However, the absence of any nickel or molybdenum oxide in NiMoAZ12 nanocatalyst suggests good dispersion of precursors of the impregnated metals over the support or the crystallite size with the lower than the XRD detection limitation.

1-2. FESEM Analysis

To investigate the effect of ZrO_2 content on catalyst morphology, FESEM images of NiMoAZx with different ZrO_2 loading are shown in Fig. 5. Loading sufficient amount of zirconia on alumina leads to the production of nanocatalysts with smaller particles and more uniform particle size distribution compared to pure alumina supported catalyst. With the addition of 5-17 wt% of ZrO_2 on alumina, the morphology of supported catalysts changes from large ensembles to smaller particles. Visible uniform morphology related to NiMoAZ12 and NiMoAZ17 nanosized catalysts micrographs can be addressed by appropriate dispersion of active metals on support. This observation is in good agreement with XRD results which were previously presented. However, increasing of ZrO_2 loading to 30 wt% resulted in particle agglomeration. As can be seen in Fig. 5(f), active metal agglomeration increased in the NiMoAZ100 nanocatalyst and formed large ensembles of particles. Active metal agglomeration causes a decrease in the number of surface metal atoms per unit mass of metal, and therefore decreases the number of active sites of the catalyst. So it can be expected that the activity of NiMoAZ30 and NiMoAZ100 nanocatalysts to be less than the other ZrO_2 containing catalysts. Zhang and coworkers [27] observed similar results after introduction of 15 wt% ZrO_2 into the alumina. They observed formation of some interpores between small particles.

Fig. 6 illustrates the particle size distribution histogram of NiMo AZ12 nanocatalyst. The quantitative investigation of FESEM image by ImageJ software shows that the particle size of NiMoAZ12 nanocatalyst is in the range of 20-80 nm with an average size of about 43 nm, which dramatically is smaller than the particle size of catalysis prepared by Zhang and coworkers [27]. Small and uniform particle size distribution of NiMoAZ12 nanocatalyst makes it a very suitable catalyst for HDS reaction.

1-3. EDX Analysis

The EDX dot-mapping images of the AZ12 support and NiMo SAZ12 nanocatalyst are illustrated in Fig. 7. All of the materials (Ni, Mo, Al, Zr, O and S) used in preparation of AZ12 and NiMoAZ12 can be observed in the EDX spectra. Some of the materials that were not detected in XRD patterns exist in EDX analysis. From the figure, homogeneous dispersion of Zr and Al oxides in AZ12 and also uniform dispersion of Ni, Mo and S elements in the form of small particles within the NiMoAZ12 nanocatalyst are observed. It is notable that high dispersion of NiMoS particles on the support can have a direct effect on the catalyst activity in HDS reaction.

1-4. BET Analysis

The BET surface areas of AZx supports and NiMoAZx nanocatalysts are shown in Fig. 8. The surface areas of γ-Al_2O_3 and pure ZrO_2 were reported 151 and 58 m^2/g, respectively. As can be seen, the specific surface area of AZx supports decreases with the increase

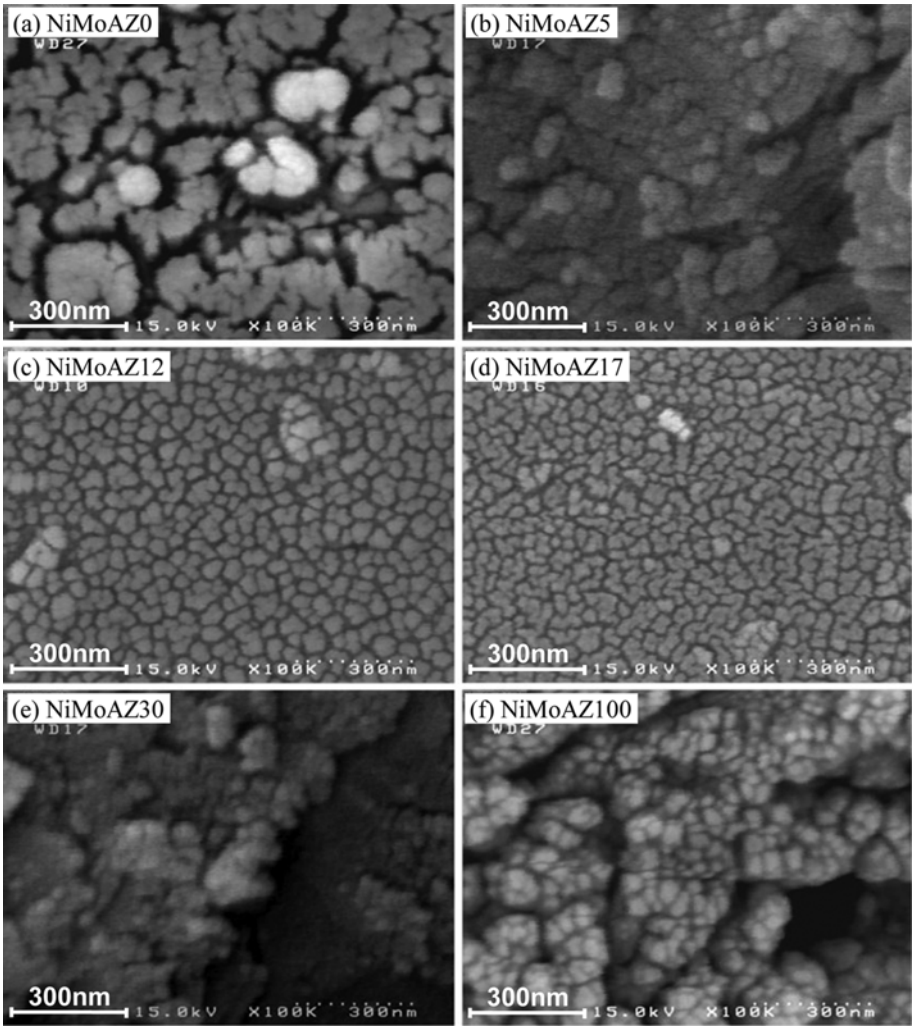

Fig. 5. FESEM images of NiMo/Al_2O_3-ZrO_2 nanocatalysts with different ZrO_2 loading: (a) NiMoAZ0, (b) NiMoAZ5, (c) NiMoAZ12, (d) NiMoAZ17, (e) NiMoAZ30 and (f) NiMoAZ100.

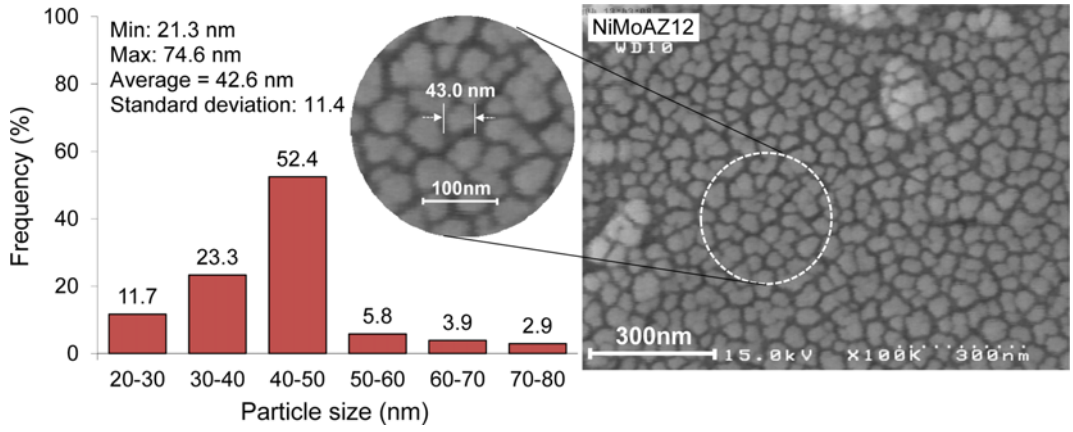

Fig. 6. Surface particle size histogram of NiMo/Al_2O_3-ZrO_2 nanocatalyst with 12 wt% ZrO_2 loading (NiMoAZ12).

in ZrO_2 loading. It can be addressed by blockage of the alumina pores by ZrO_2 particles. According to the literature [40], loading even a small amount of zirconia on alumina causes a decrease in surface area and when zirconia crystal phase begins to appear, the surface area decreases below 100 m^2/g. On the other hand Klimova [41] and coworkers observed for catalysis synthesized via sol gel methods the surface area increases by loading of zirconia up to 50 %.wt.; further loading of zirconia decreases it. The results also show that incor-

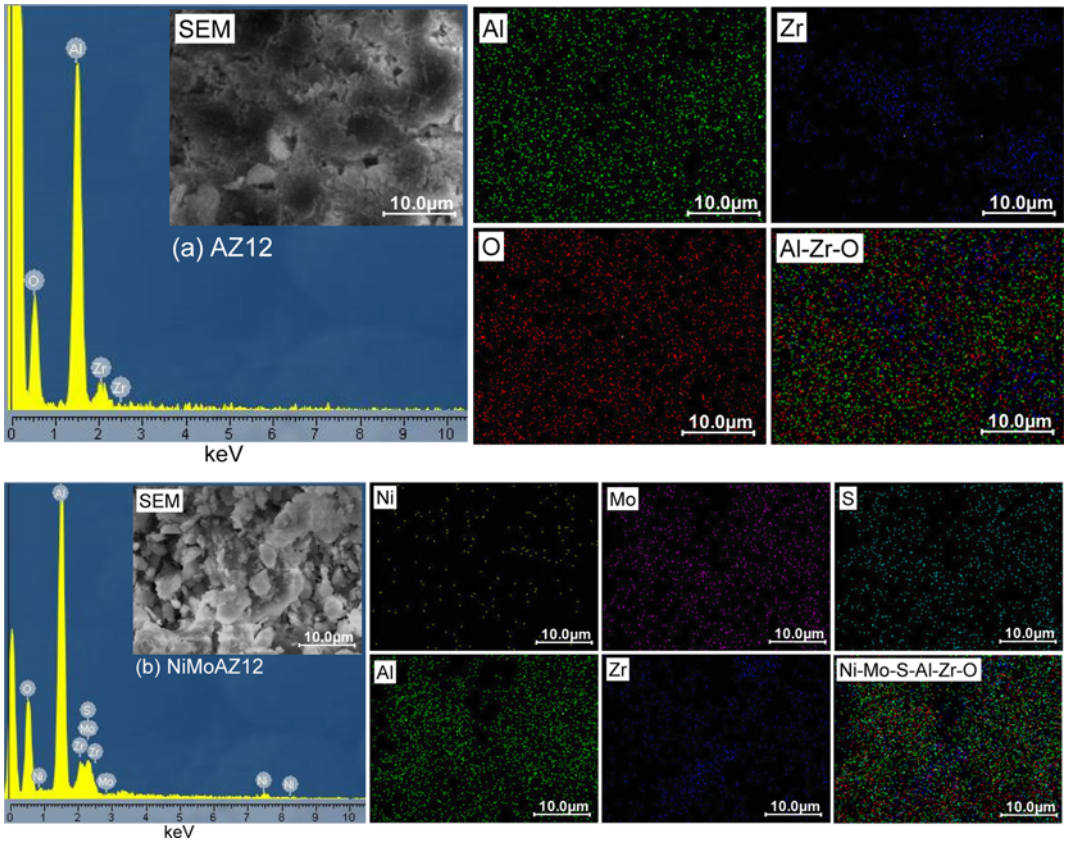

Fig. 7. EDX analysis of Al_2O_3-ZrO_2 support and $NiMo/Al_2O_3$-ZrO_2 nanocatalyst (a) AZ12 and (b) NiMoAZ12.

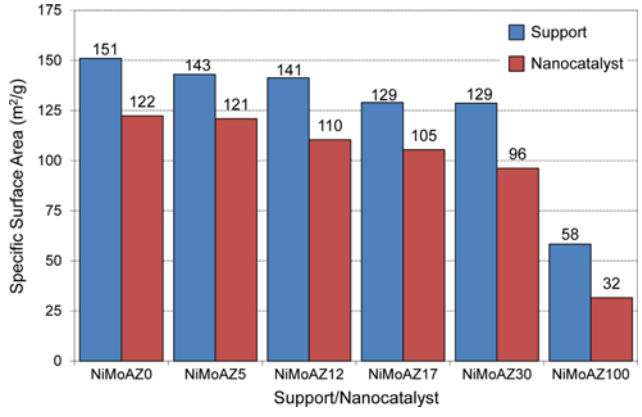

Fig. 8. BET surface area of synthesized support and $NiMo/Al_2O_3$-ZrO_2 nanocatalysts with different ZrO_2 loading.

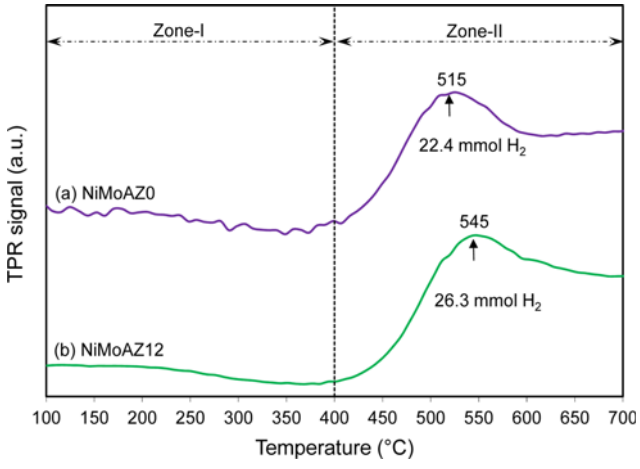

Fig. 9. TPR-H_2 analysis of Al_2O_3-ZrO_2 support and $NiMo/Al_2O_3$-ZrO_2 nanocatalyst (a) NiMoAZ0 and (b) NiMoAZ12.

poration of molybdenum and nickel into AZx support causes a decrease in surface area of the samples. That can be addressed by deposition of Ni and Mo particles in the pores of support.

1-5. TPR-H_2 Analysis

Temperature programmed reduction (TPR-H_2) analysis was performed on NiMoAZ0 and NiMoAZ12 nanocatalysts to address the interaction between active metal and support (Fig. 9). The reduction peaks are reported about 515 and 545 °C for NiMoAZ0 and NiMoAZ12 nanocatalysts, respectively. Variation of TPR-H_2 profiles indicates that the nature of surface molybdenum and nickel species in $NiMo/Al_2O_3$ changed with loading of ZrO_2 (12 wt%). Due to the broadness of TPR-H_2 profiles, it is not possible to distinguish the nature of Ni and Mo species. The higher amount of hydrogen consumption corresponding to NiMoAZ12 compared that corresponding to the NiMoAZ0, and consequently higher reducibility of NiMoAZ12 catalyst may arise as a result of relatively weaker metal-support interaction in this sample that is favorable in HDS reaction [27]. According to ref. [42] the introduction of ZrO_2 into the alumina changed the TPR pattern via these two ways: (i) increas-

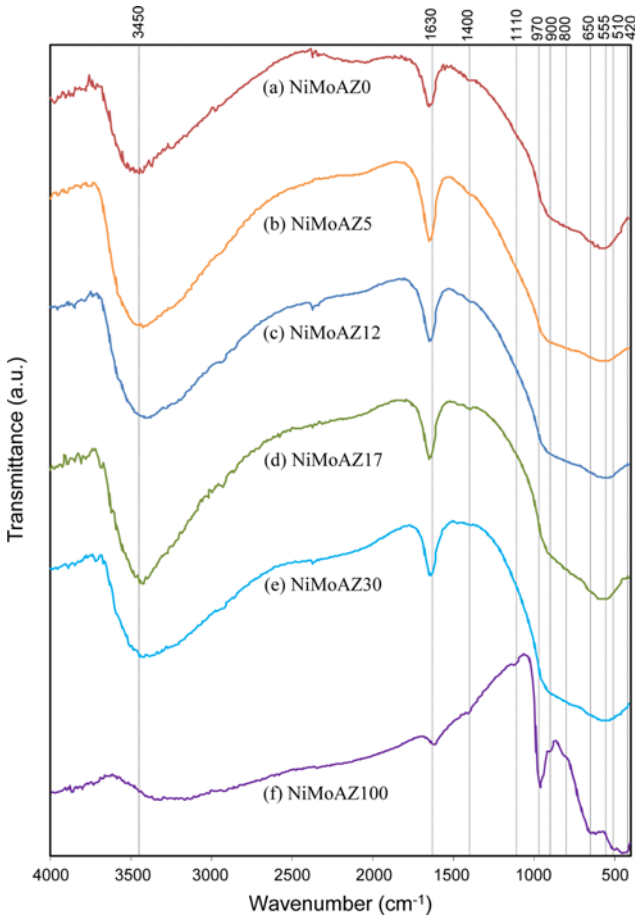

Fig. 10. FTIR spectra of NiMo/Al_2O_3-ZrO_2 nanocatalysts with different ZrO_2 loading: (a) NiMoAZ0, (b) NiMoAZ5, (c) NiMo AZ12, (d) NiMoAZ17, (e) NiMoAZ30 and (f) NiMoAZ100.

ing the amount of consumed hydrogen, and (ii) decreasing of reduction temperature. In the case of our study, TPR profiles show higher amount of hydrogen consumption correspond to NiMoAZ12 in comparison with the NiMoAZ0. This observation indicates that incorporation of ZrO_2 on support leads to an increase in the number of active species in the NiMo catalyst which have adequate interaction with support and are able to be reduced at relatively low temperature range (below 700). This result is in good agreement with ref. [23]

1-6. FTIR Analysis

Fig. 10 shows the FTIR spectra of the NiMoAZx catalysts in the range of 400-4,000 cm^{-1}. The peaks at 1,630 and 3,450 cm^{-1} are assigned to the bending and stretching vibrations of the O-H bond due to absorbed water molecules [43-46]. The spectrum of the samples with alumina and mixed oxide supports shows a broad vibration centered near 555 cm^{-1} which is attributed to Al-O [47-49]. FTIR spectra of NiMoAZ100 are different from other samples and shows peaks at 970, 460 and 510 cm^{-1}. The peak at 970 cm^{-1} corresponds to the metal=oxygen bond that in our investigation can be related to the stretching vibration of Mo=O. The bands at wave numbers around 460 and 510 cm^{-1} are ascribed to Zr-O vibrations of tetragonal phase of ZrO_2 [50-52]. It is notable that no vibrating bands corresponding to zirconia phase were registered in mixed

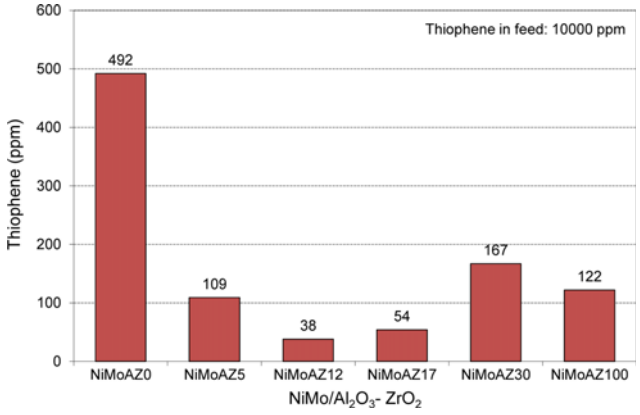

Fig. 11. Catalytic performance of NiMo/Al_2O_3-ZrO_2 nanocatalysts with different ZrO_2 loading toward hydrodesulfurization of thiophene.

oxides supported catalysts spectra. This observation is attributed to non-crystalline nature of ZrO_2 in these samples and complements the XRD results.

2. Catalytic Performance Study in Hydrodesulfurization Reaction

The catalytic activities in hydrodesulfurization of thiophene were evaluated on the sulfided catalysts as functions of support composition and the results are shown in Fig. 11. Obviously, the introduction of ZrO_2 to NiMo/Al_2O_3 enhances the HDS activity. As can be seen, the ZrO_2-doped supported catalysts exhibit much higher thiophene conversion than the pure alumina supported catalyst. The maximum activity was observed for NiMoAZ12 nanocatalyst, which was predicted from characterization results. The reaction over this nanocatalyst decreased the sulfur content of feed from 10,000 to 38 ppm. Excellent activity of the NiMoAZ12 nanocatalyst can be attributed to small and uniform particle size distribution as well as relatively higher reducibility. Thiophene conversion decreases with the further increase of ZrO_2 content, but it still remains slightly higher than the Al_2O_3 supported catalyst. For catalysts prepared over the AZ30 and AZ100 supports, the significant decrease

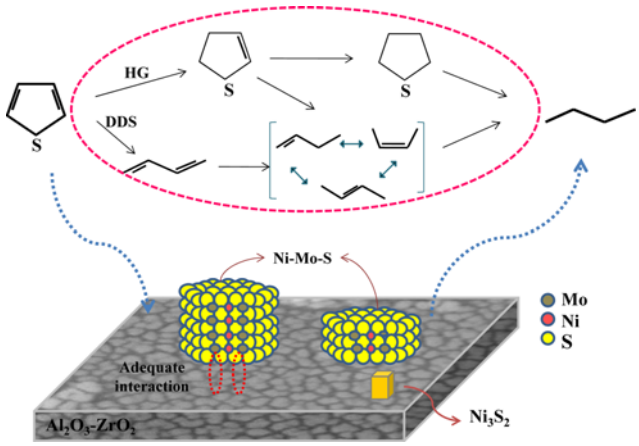

Fig. 12. Reaction mechanism of thiophene hydrodesulfurization over NiMo/Al_2O_3-ZrO_2 nanocatalyst.

in activity can be explained by active metal agglomeration and reduction in surface area which resulted from FESEM and BET results, respectively.

3. Hydrodesulfurization Reaction Mechanism

The reaction scheme of thiophene hydrodesulfurization over NiMo/Al_2O_3-ZrO_2 nanocatalysts is shown in Fig. 12. According to literature [53,54] the reaction of thiophene with H_2 over sulfided catalysts occurs via two parallel pathways:

(a) Hydrogenation of the aromatic ring of thiophene to tetrahydrothiophene, with further C-S bonding hydrogenolysis leading to butane.

(b) Direct C-S scission to form 1,3-butadiene which is lately hydrogenated to form butene.

1-Butene, cis- and trans-2-butene are intermediary products that can be hydrogenated to form n-butane. In hydrodesulfurization of thiophene, it is almost impossible to discriminate between those pathways from product yields, as butadiene produced via DDS pathway is rapidly hydrogenated to butene and butane, the product of HG [53]. It has been found that the formation of NiMoS active sites is necessary to provide the catalyst ability for the cleavage of the C-S bond in the thiophene molecule [54]. The improvement in the overall HDS activity of thiophene over Al_2O_3-ZrO_2 supported catalyst suggests the formation of greater number of Ni-Mo-S active sites. There are two distinct types of active sites for adsorption of thiophene. One site is proposed to catalyze direct C-S cleavage through the involvement of sulfur vacancies (coordinately unsaturated sites) at edges of the NiMoS structures. The other site that occurs on the top of NiMoS slabs, close to the edges, catalyzes the hydrogenation and hydrogenolysis of C-C and C-S bonds [55].

CONCLUSIONS

The introduction of proper amount of ZrO_2 into Al_2O_3 matrix combines the favorable properties of both components. Therefore, NiMo/Al_2O_3-ZrO_2 nanocatalyst with optimum content of ZrO_2 can be a promising catalyst for hydrodesulfurization process. The optimum value of ZrO_2 was found to be 12 wt%. Introduction of this amount of ZrO_2 into alumina leads to the formation of nanostructured catalyst with smaller and more uniform particle size distribution. Adequate interaction between active metals and support in NiMo/AZ12 nanocatalyst seems to be responsible for the obtained relative maximum hydrodesulfurization activity.

ACKNOWLEDGEMENTS

The authors gratefully acknowledge Sahand University of Technology for the financial support of the research as well as Iran Nanotechnology Initiative Council for complementary financial supports.

REFERENCES

1. F. Rashidi, T. Sasaki, A. M. Rashidi, A. Nemati Kharat and K. J. Jozani, *J. Catal.*, **299**, 321 (2013).
2. H. Song, J. Wang, Z. Wang, H. Song, F. Li and Z. Jin, *J. Catal.*, **311**, 257 (2014).
3. P. A. Nikulshin, V. A. Salnikov, A. V. Mozhaev, P. P. Minaev, V. M. Kogan and A. A. Pimerzin, *J. Catal.*, **309**, 386 (2014).
4. S. Aghamohammadi, M. Haghighi and S. Karimipour, *J. Nanosci. Nanotechnol.*, **13**, 4872 (2013).
5. M. Khatamian, A. A. Khandar, M. Haghighi, M. Ghadiri and M. Darbandi, *Powder Technol.*, **203**, 503 (2010).
6. D. Wang, X. Li, E. W. Qian, A. Ishihara and T. Kabe, *Appl. Catal., A*, **238**, 109 (2003).
7. R. Leliveld, A. Van Dillen, J. Geus and D. Koningsberger, *J. Catal.*, **165**, 184 (1997).
8. N. Azizi, S. A. Ali, K. Alhooshani, T. Kim, Y. Lee, J.-I. Park, J. Miyawaki, S.-H. Yoon and I. Mochida, *Fuel Process. Technol.*, **109**, 172 (2013).
9. X. Li, D. Han, Y. Xu, X. Liu and Z. Yan, *Mater. Lett.*, **65**, 1765 (2011).
10. Y. Fan, G. Shi, H. Liu and X. Bao, *Fuel*, **90**, 1717 (2011).
11. R. Huirache-Acuña, R. Nava, C. L. Peza-Ledesma, J. Lara-Romero, G. Alonso-Núez, B. Pawelec and E. M. Rivera-Muñoz, *Materials*, **6**, 4139 (2013).
12. A. Stanislaus, A. Marafi and M. S. Rana, *Catal. Today*, **153**, 1 (2010).
13. D. Valencia and T. Klimova, *Catal. Today*, **166**, 91 (2011).
14. S. K. Maity, M. S. Rana, B. N. Srinivas, S. K. Bej, G. Murali Dhar and T. S. R. Prasada Rao, *J. Mol. Catal. A: Chem.*, **153**, 121 (2000).
15. M. Jia, P. Afanasiev and M. Vrinat, *Appl. Catal., A*, **278**, 213 (2005).
16. J. Mazurelle, C. Lamonier, C. Lancelot, E. Payen, C. Pichon and D. Guillaume, *Catal. Today*, **130**, 41 (2008).
17. H. Song, M. Dai, H. Song, X. Wan, X. Xu, C. Zhang and H. Wang, *Catal. Commun.*, **43**, 151 (2014).
18. M. J. Vissenberg, Y. van der Meer, E. J. M. Hensen, V. H. J. de Beer, A. M. van der Kraan, R. A. van Santen and J. A. R. van Veen, *J. Catal.*, **198**, 151 (2001).
19. M. Kouzu, Y. Kuriki, F. Hamdy, K. Sakanishi, Y. Sugimoto and I. Saito, *Appl. Catal., A*, **265**, 61 (2004).
20. H. Shang, C. Liu, Y. Xu, J. Qiu and F. Wei, *J. Nat. Gas Chem.*, **15**, 203 (2006).
21. U. T. Turaga and C. Song, *Catal. Today*, **86**, 129 (2003).
22. M. Hussain, S.-K. Song and S.-K. Ihm, *Fuel*, **106**, 787 (2013).
23. T. E. Klimova, D. Valencia, J. A. Mendoza-Nieto and P. Hernández-Hipólito, *J. Catal.*, **304**, 29 (2013).
24. S. Damyanova, M. A. Centeno, L. Petrov and P. Grange, *Spectrochim. Acta, Part A*, **57**, 2495 (2001).
25. S. Damyanova, L. Petrov, M. A. Centeno and P. Grange, *Appl. Catal., A*, **224**, 271 (2002).
26. S. Damyanova, P. Grange and B. Delmon, *J. Catal.*, **168**, 421 (1997).
27. D. Zhang, A. Duan, Z. Zhao, G. Wan, Z. Gao, G. Jiang, K. Chi and K. H. Chuang, *Catal. Today*, **149**, 62 (2010).
28. G. Li, W. Li, M. Zhang and K. Tao, *Catal. Today*, **93-95**, 595 (2004).
29. G. Li, W. Li, M. Zhang and K. Tao, *Appl. Catal., A*, **273**, 233 (2004).
30. C. Pophal, F. Kameda, K. Hoshino, S. Yoshinaka and K. Segawa, *Catal. Today*, **39**, 21 (1997).
31. J. R. Grzechowiak, I. Wereszczako-Zielińska and K. Mrozińska, *Catal. Today*, **119**, 23 (2007).
32. H. Song, M. Dai, Y.-T. Guo and Y.-J. Zhang, *Fuel Process. Technol.*, **96**, 228 (2012).
33. Y. Vafaeian, M. Haghighi and S. Aghamohammadi, *Energy Convers. Manage.*, **76**, 1093 (2013).
34. M. S. Ghodrati, M. Haghighi, J. S. Soltan Mohammadzadeh, B. Pourabas and E. Pipelzadeh, *Reac. Kin. Mech. Catal.*, **104**, 49 (2011).

35. R. Khoshbin, M. Haghighi and N. Asgari, *Mater. Res. Bull.*, **48**, 767 (2013).
36. R. Khoshbin and M. Haghighi, *Catal. Sci. Technol.*, **4**, 1779 (2014).
37. J. Baneshi, M. Haghighi, N. Jodeiri, M. Abdollahifar and H. Ajamein, *Energy Convers. Manage.*, **87**, 928 (2014).
38. S. Allahyari, M. Haghighi, A. Ebadi, S. Hosseinzadeh and H. Gavam Saeedi, *Reac. Kin. Mech. Catal.*, **112**, 101 (2014).
39. J. M. Dominguez, J. L. Hernandez and G. Sandoval, *Appl. Catal., A*, **197**, 119 (2000).
40. E. Liu, A. J. Locke, R. L. Frost and W. N. Martens, *J. Mol. Catal. A: Chem.*, **353-354**, 95 (2012).
41. T. Klimova, M. L. Rojas, P. Castillo, R. Cuevas and J. RamÃ-rez, *Micropor. Mesopor. Mater.*, **20**, 293 (1998).
42. M. A. Al-Daous and S. A. Ali, *Fuel*, **97**, 662 (2012).
43. N. Rahemi, M. Haghighi, A. A. Babaluo, M. F. Jafari and P. Estifaee, *J. Ind. Eng. Chem.*, **19**, 1566 (2013).
44. R. Khoshbin and M. Haghighi, *Chem. Eng. Res. Des.*, **91**, 1111 (2013).
45. S. Saedy, M. Haghighi and M. Amirkhosrow, *Particuology*, **10**, 729 (2012).
46. Z. Abbasi, M. Haghighi, E. Fatehifar and N. Rahemi, *Asia-Pac. J. Chem. Eng.*, **7**, 868 (2012).
47. A. Sharma, S. Kumar, N. Budhiraja, R. Singh and M. Singh, *Adv. App. Sci. Res.*, **4**, 252 (2013).
48. F. Rahmani, M. Haghighi and P. Estifaee, *Micropor. Mesopor. Mater.*, **185**, 213 (2014).
49. S. Allahyari, M. Haghighi, A. Ebadi and S. Hosseinzadeh, *Ultrason. Sonochem.*, **21**, 663 (2014).
50. M. C. Barrera, J. Escobar, J. A. de los Reyes, M. A. Cortés, M. Viniegra and A. Hernández, *Catal. Today*, **116**, 498 (2006).
51. A. Taavoni-Gilan, E. Taheri-Nassaj, R. Naghizadeh and H. Akhondi, *Ceram. Int.*, **36**, 1147 (2010).
52. J. R. Sohn, E. W. Chun and Y. I. Pae, *Bull. Korean Chem. Soc.*, **24**, 1785 (2003).
53. N. Kagami, *Advances in HDS catalysts design: relation between catalyst structure and feed composition*, Delft University of Technology, Netherlands (2006).
54. D. Valencia, I. García-Cruz and T. Klimova, *Effect of citrate addition in NiMo/SBA-15 catalysts on selectivity of DBT hydrodesulfurization*, In *Studies in Surface Science and Catalysis*, E. M. Gaigneaux, M. D. S. H. P. A. J. J. A. M. and Ruiz, P., Eds., Elsevier, **175**, 529 (2010).
55. H. Wang and E. Iglesia, *J. Catal.*, **273**, 245 (2010).